ELSEVIER

Chemical Physics 252 (2000) 323–335

Chemical Physics

www.elsevier.nl/locate/chemphys

Effect of collisions on the orientational relaxation of photofragments

A.P. Blokhin *, M.F. Gelin

Institute of Molecular and Atomic Physics, National Academy of Sciences of Belarus, Skaryna pr.70, Minsk, 220072, Belarus

Received 21 July 1998

Abstract

Effect of collisions is investigated on the photofragment anisotropy decay. We restrict ourselves to studying linear fragments, and no rotational predissociation is assumed. Photoproducts are produced with a nonequilibrium rotational distribution, basically due to the applied torque and the parent molecule rotation. A kinetic equation, describing rotational relaxation of linear fragments under nonequilibrium conditions, is derived and solved for angular momentum correlation functions (CFs), rotational energy CFs, and also orientational CFs (OCFs). The characteristic decay times for the angular momentum and rotational energy CFs are shown to be insensitive to the mechanism of the photofragmentation. On the contrary, OCF of the second rank, that completely determines anisotropy of the photoproduct emission, is demonstrated to be very sensitive to peculiarities of the dissociation process and collision dynamics. This is confirmed by comparison of the calculated photoproduct anisotropies with experimental [M. Volk, S. Gnanakaran, E. Gooding, Y. Kholodenko, N. Pugliano, R.M. Hochstrasser, J. Phys. Chem. A 101 (1997) 638] and simulated [I. Benjamin, U. Banin, S. Ruhman, J. Chem. Phys. 98 (1993) 8337] ones. The fragment ensemble is proved to retain some memory about its initial nonequilibrium distribution. This pertains not only to the short time behavior for the anisotropy, but also for its long time decay. Therefore, the study of the polarization response of the ensemble of photoproducts allows one to know about features of the photofragmentation dynamics, and also to get information about peculiarities of collisions of fragments with buffer medium species.

Keywords: Photodissociation in solutions; Polarization response; Orientational relaxation

1. Introduction

Ensemble of products produced through the photofragmentation of an ensemble of parent molecules is rotationally and orientationally anisotropic [1,2]. Schematically, this anisotropy has both optical and dynamic origin. The former is due to the fact that the probability of absorption and/or emission of light is proportional to $(\vec{e}\,\vec{\mu})^2$, with $\vec{e}$ being the light polarization and $\vec{\mu}$ being the transition dipole moment. The latter is a direct consequence of the observation that rotational excitation of fragments is determined by the parent molecule geometry and peculiarities of the dissociation process. That is why the investigation of the anisotropy of the photoproduct emission allows one to know about the photofragmentation mechanism in considerable detail. Traditionally, experimental and theoretical efforts were directed to studying the steady state ani-

* Corresponding author. Fax: +7-375-0172-840-030; E-mail: 1sfm@imaph.bas-net.by

0301-0104/00/$ - see front matter
PII: S0301-0104(99)00360-2

sotropy, both for diatomic [1–17] and polyatomic [18,19] fragments. The advent of the femtosecond polarization spectroscopy made it possible to monitor the fragment anisotropy decay in real time [20–22]. However, these experiments (both in the steady state and in the time domain) have been performed in the gas phase under collision free conditions, where the main source of the anisotropy decay is due to the free rotation of products. On the other hand, a collisional environment is a natural medium for the majority of photoreactions, including those of biological significance [23–25]. Recently, a number of 'real time' measurements [24–32] and computer simulations [23,33–36] was reported, where the anisotropy decay of diatomic photoproducts was studied in the condensed phase.

Evidently, intermolecular collisions destroy the initially produced nonequilibrium distribution. So, the natural question arises: 'Whether is it possible to extract information about the photofragmentation dynamics by monitoring the photoproduct anisotropy decay, or a few collisions are enough to maintain an equilibrium distribution so that the observed data reflect orientational relaxation under equilibrium conditions?' On the other hand, our knowledge about rotational and orientational relaxation in gases and liquids is due to the numerous spectroscopic experiments and computer simulations. The great bulk of these studies was carried out under equilibrium conditions [37–41]. Fragments produced through the photolysis of parent molecules have a nonequilibrium, nonthermal rotational distribution. So, the study of the relaxation of such nonequilibrim distribution to an equilibrium one will provide us with a crucial test for a collision model invoked for the description of intermolecular collisions.

The present work is aimed at presenting a relatively simple model for the description of the photoproduct anisotropy decay due to intermolecular collisions. The model contains a few parameters with a clear-cut physical meaning. This makes it convenient enough for the interpretation of results of experiments and simulations. We restrict ourselves to studying linear parent and product molecules, that mimics dissociation of a triatomic molecule into a diatomic and an atom. The photofragment distribution over angular momenta is derived in Section 2. The kinetic equations governing the collisional relaxation of the nonequilibrium distribution are introduced in Section 3 and solved for the angular momentum, rotational energy correlation functions (CFs), and orientational CFs (OCFs) of the second rank. The obtained results are discussed in Section 4, where our theoretical predictions are tested against experimental results [31] and computer simulations [34]. In Section 5, which is the Conclusion, the essence of the work is summarized.

Note that the rotational predissociation is ignored in the subsequent analyses. This assumption is obeyed quite well for at least dissociation of a number of triatomics [20–22,26–36]. If necessary, predissociation can also be included into consideration by an appropriate generalization of the results of papers [42] to collisional environments.

2. Photoproduct angular momentum distribution

We consider the photofragmentation dynamics in the reaction $A + h\upsilon \rightarrow B +$ products under the following assumptions [19,22,42–46]:

- molecules A and B are rigid tops,
- photofragmentation proceeds instantaneously,
- classical mechanics is an adequate description of the process.

The most crucial assumption here is that concerning the promptness of the photofragmentation. It fulfils quite well on the time scale of molecular rotation. Indeed, a characteristic time for the rotational reorientation $\tau_r \approx \sqrt{I/kT} \approx 1.1\sqrt{I/T}$ ps. Here I is the main moment of inertia in a.u. Å^2, and T is the rotational temperature in kelvins. So, at a room temperature, τ_r falls normally into the picosecond time region. On the other hand, the photofragmentation time was estimated to be as small as 50–200 fs [20–22,26–36]. There exist two basic sources for the rotational excitation of photoproducts, viz. the torque due to the rapture of chemical bonds and the parent molecule rotation. By using the assumptions mentioned above and the angular momentum conservation low one can establish the following relationship between the parent and product angular momenta [19,22,42–46]:

$$\vec{J}_B = G\vec{J}_A + \vec{\Delta}. \qquad (1)$$

Here the first summand describes mapping of the parent angular momentum into the product one, and the second summand is merely the additional angular momentum ascribed by the product due to the torque. Explicitly,

$$G_{ab} = I_{B,a} R_{ab}(\Xi)\, I_{A,b}, \tag{2}$$

with $I_{B,a}$ and $I_{A,b}$ being the main moments of inertia of molecules A and B, $R_{ab}(\Xi)$ being the matrix of rotation from the frame of the main moments of inertia of B to that of A, and Ξ are the pertinent Euler angles. While the direction of $\vec{\Delta}$ is known ($\vec{\Delta}$ is conventionally assumed to be pointed along the direction of the ruptured bond), one can invoke the energy balance to estimate the magnitude of $\vec{\Delta}$, as it is conventionally done in the impulsive models [22].

Being specialized to the case when A and B are linear rotors with their axes being parallel to each other ($\Xi = 0$), Eq. (1) reduces to

$$\vec{J}_B = (I_B/I_A)\,\vec{J}_A + \vec{\Delta}, \tag{3}$$

where $\vec{J}_B, \vec{J}_A, \vec{\Delta}$ are the two-dimensional vectors. By assuming that the parent molecules possess a Boltzmann equilibrium distribution at the temperature T^A, one arrives at the following distribution over the photofragment angular momenta:

$$\rho_0\left(\vec{J}_B\right) = (\eta/\pi)\exp\left\{-\eta\left(\vec{J}_B - \vec{\Delta}\right)^2\right\},$$

$$\eta \equiv I_A/\left(2kT_A I_B^2\right), \tag{4}$$

(compare with Refs. [47–49]). This is evidently a Gaussian but not a Boltzmann distribution. It is centered in the vicinity of $\vec{J}_B = \vec{\Delta}$. For the further implementation of distribution (4) one should invoke symmetry arguments. While a triatomic molecule dissociates from a bent configuration, a diatomic fragment is produced with an additional angular momentum $\vec{\Delta}$, either due to the applied torque or the recoil of a heavy atom. In any case, there is no preferential orientation of $\vec{\Delta}$ in the photoproduct frame. Therefore, Eq. (4) should be averaged over all possible directions of $\vec{\Delta}$. This can immediately be done by introducing the polar coordinates

$$J_x = J\cos\varphi_J,\ J_y = J\sin\varphi_J;$$

$$\Delta_x = \Delta\cos\varphi_\Delta,\ \Delta_y = \Delta\sin\varphi_\Delta. \tag{5}$$

and integrating Eq. (4) over φ_Δ:

$$\rho_0(J) = (2\pi)^{-1}\int_0^{2\pi} d\varphi_\Delta\ \rho_0\left(\vec{J}\right) = (\eta/\pi)\, I_0(2\eta J\Delta)\exp\left\{-\eta(J^2+\Delta^2)\right\}, \tag{6}$$

where

$$I_0(z) = \sum_{k=0}^{\infty}\frac{(z^2/4)^k}{(k!)^2} \tag{7}$$

is the modified Bessel function. This is the distribution which is implemented in all the subsequent calculations. It depends only on $|\vec{J}|$ and is centered near $J = \Delta$. Hereafter, the subscript B, denoting the fragment angular momenta, is omitted for brevity.

3. Rotational and orientational CFs

The standard kinetic equation for describing rotational motion of linear molecules reads as follows [40,50,51]:

$$\partial_t \rho\left(\vec{J},\Omega,t\right) = -\left\{i I_B^{-1}\vec{J}\hat{\vec{J}}(\Omega) + z_c\right\}\rho\left(\vec{J},\Omega,t\right) + z_c\int d\vec{J}'\, T\left(\vec{J}|\vec{J}'\right)\rho\left(\vec{J}',\Omega,t\right). \tag{8}$$

Here $\vec{J}$ is the (two-dimensional) angular momentum in the molecular frame, the Euler angles Ω specify orientation of the molecular frame with respect to the laboratory one, $\hat{\vec{J}}(\Omega)$ is the angular momentum operator in the molecular frame, and z_c is the collision frequency. To describe the collision dynamics we chose the Keilson–Storer kernel [52]:

$$T\left(\vec{J}|\vec{J}'\right) = \left[2\pi I_B kT_{eq}(1-\gamma^2)\right]^{-1} \times\exp\left\{-\left(\vec{J}-\gamma\vec{J}'\right)^2 / \left[2I_B kT_{eq}(1-\gamma^2)\right]\right\}, \tag{9}$$

with T_{eq} being the (equilibrium) rotational temperature of the buffer medium. It is evident that generally $T_{eq} \neq T_A$. The parameter $-1 \le \gamma \le 1$ specifies the collision process. When $\gamma = 1$, $T(\vec{J}|\vec{J}') \to \delta(\vec{J}-\vec{J}')$, the angular momentum is conserved, and Eq. (8)

reduces to the free rotor Liouville equation. Provided that $\gamma = 0$, intermolecular interactions are so strong that a single collision is enough to establish a Boltzmann equilibrium distribution: $T(\vec{J}|\vec{J}') \to \rho_{eq}(\vec{J})$

$$\rho_{eq}(\vec{J}) = (2\pi I_B kT_{eq})^{-1} \exp\left\{-\vec{J}^2/(2I_B kT_{eq})\right\}. \tag{10}$$

By letting $\gamma = -1$, one gets $T(\vec{J}|\vec{J}') \to \delta(\vec{J}+\vec{J}')$, so that the angular momentum is reversed due to a collision. Eq. (8) with kernel (9) contains, as a special case, the J-diffusion model ($\gamma = 0$) [40,50,53] and the rotational Fokker–Planck equation ($z_c \to \infty, \gamma \to 1, z_c(1-\gamma) \to \nu_J = \text{const}$) [40,50,51,53]. If $0 \le \gamma \le 1$ the Keilson–Storer model interpolates smoothly between these two models, and generalizes the approaches to the description of the preferential reorientation of the angular momentum in the course of collisions. The Keilson–Storer kernel obeys the detailed balance conditions

$$T(\vec{J}|\vec{J}')\rho_{eq}(\vec{J}') = T(\vec{J}'|\vec{J})\rho_{eq}(\vec{J}). \tag{11}$$

The requirement ensures relaxation of an arbitrary initial distribution to the equilibrium one (10). Kinetic Eq. (8) with the Keilson–Storer kernel (9) has extensively been studied in the literature in case of an equilibrium initial conditions, i.e., $\rho(\vec{J},\Omega,t=0) = \rho_{eq}(\vec{J})$ [40,54,55]. However, the photogragmentation process manifests itself in the nonequilibrium initial conditions (6), i.e., $\rho(\vec{J},\Omega,t=0) = \rho_0(\vec{J})$. To calculate the rotational and orientational CFs under these nonequilibrium conditions is the goal of the present section.

By simply multiplying Eq. (8) by J_α and $J_\alpha J_\beta$, one can immediately calculate the angular momentum and rotational energy CFs:

$$\langle \vec{J}(0)\vec{J}(t)\rangle = \exp\{-\nu_J t\}\langle \vec{J}^2\rangle,$$

$$\langle \vec{J}^2\rangle = \Delta^2 + \eta^{-1}; \tag{12}$$

$$\langle \vec{J}^2(t)\rangle = \langle \vec{J}^2\rangle + \exp\{-\nu_E t\}\left(\langle \vec{J}^2\rangle - \langle \vec{J}^2\rangle_{eq}\right) \tag{13}$$

$$\langle \vec{J}^2(0)\vec{J}^2(t)\rangle = \langle \vec{J}^2\rangle\langle \vec{J}^2\rangle_{eq} + \exp\{-\nu_E t\} \times \left(\langle \vec{J}^4\rangle - \langle \vec{J}^2\rangle\langle \vec{J}^2\rangle_{eq}\right), \tag{14}$$

$$\langle \vec{J}^4\rangle = 2\eta^{-2} + 4\eta^{-1}\Delta^2 + \Delta^4,\ \langle \vec{J}^2\rangle_{eq} = 2I_B kT_{eq};$$
$$\nu_J \equiv \tau_J^{-1} = z_c(1-\gamma),\ \nu_E \equiv \tau_E^{-1} = z_c(1-\gamma^2). \tag{15}$$

So, the angular momentum and rotational energy CFs exhibit simple exponential damping with the decay times τ_J and τ_E (15), identically as in case of an equilibrium initial distribution [40]. So the characteristic decay times are not sensitive to the mechanism of the photofragmentation. Only the averaged values of even moments of $\vec{J}$ do depend on η and Δ. On the contrary, as it is demonstrated below, OCFs are very sensitive to the peculiarities of the dissociation process.

OCFs are defined as follows:

$$G_{kn}^j(t) \equiv \int d\vec{J} G_{kn}^j(\vec{J},t) \equiv \sum_{m=-j}^{j} \langle D_{km}^j(-\Omega(0)) D_{mn}^j(\Omega(t))\rangle, \tag{16}$$

where $D_{mn}^j(\Omega)$ are the Wigner D-functions. Under the certain assumptions [18–35], anisotropy of the photoproduct emission is determined by the second rank OCF:

$$r(t) = 2/5\langle P^2(\vec{\mu}_1(0)\vec{\mu}_2(t))\rangle = 2/5 \sum_{k,l=-2}^{2} D_{0k}^2(-\vec{\mu}_1) G_{kl}^2(t) D_{l0}^2(\vec{\mu}_2), \tag{17}$$

with $\vec{\mu}_1$ and $\vec{\mu}_2$ being the unit vectors along the pump and probe transitions. On inserting definition (16) into Eq. (8), one arrives at the following kinetic equation for OCFs:

$$\partial_t G_{kl}^j(\vec{J},t) = -i \sum_{m=-j}^{j} \vec{J}\vec{J}_{km}^j G_{ml}^j(\vec{J},t) - z_c G_{kl}^j(\vec{J},t) + z_c \int d\vec{J}'\, T(\vec{J}|\vec{J}') G_{kl}^j(\vec{J},t), \tag{18}$$

$$G_{kl}^j(\vec{J},t=0) = \rho_0(J)\delta_{kl}^j. \tag{19}$$

Here

$$J^j_{x,kl} \pm J^j_{y,kl} = \delta^j_{k,l\mp 1}\sqrt{(j\pm l)(j\mp l+1)}\,,$$

$$J^j_{z,kl} = \delta^j_{kl}, -j \le k,l \le j\,, \qquad (20)$$

are the matrix elements of the angular momentum operators over the *D*-functions. Hereafter, dimensionless variables are used throughout the article: time is measured in units $\sqrt{I_B/kT_{eq}}$ and angular momenta in $\sqrt{I_B kT_{eq}}$. In these new variables

$$\eta \equiv I_A T_{eq}/(2T_A I_B)\,,$$

$$\rho_{eq}(\vec{J}) \equiv (2\pi)^{-1}\exp\left(-\vec{J}^2/2\right). \qquad (21)$$

Eq. (18) with nonequilibrium distribution (19) can easily be solved analytically in the rarefied gas ($z_c = 0$) and in the diffusive ($z_c \gg 1$) limit. In the former case, one should merely average the free linear rotor OCF [56]

$$F^j_{kn}(\vec{J},t) = \sum_{m=-j}^{j} \mathrm{d}^j_{km}(-\pi/2)\mathrm{d}^j_{mn}(\pi/2) \times \exp\{-\mathrm{i}\varphi_j(n-k) - \mathrm{i}mJt\}\,. \qquad (22)$$

over the nonequilibrium distribution (6) (see also Refs. [20–22]). The result reads

$$z_c = 0 \Rightarrow G^j_{kl}(t) = G^j_k(t)\,\delta^j_{kl}\,,$$

$$G^j_k(t) = \left(\mathrm{d}^j_{00}(\pi/2)\right)^2 + \int_0^\infty J\mathrm{d}J\rho_0(J) \times \sum_{m=1}^{j}\left(\mathrm{d}^j_{mk}(\pi/2)\right)^2\cos(mJt)\,. \qquad (23)$$

By applying the projection operator technique [57,58] to Eq. (18), one finds that in the diffusion limit the standard small angle rotational diffusion [40,50–55,57,58] takes place, irrespectively of the particular form of distribution (19):

$$z_c \gg 1 \Rightarrow G^j_{kl}(t) = G^j_k(t)\,\delta^j_{kl},$$

$$G^j_k(t) = \exp\{-t\tau_J(j(j+1)-k^2)\}\,. \qquad (24)$$

The result is quite obvious, since angular momenta are quick variables in the diffusion limit ($\tau_J \ll 1$). So, any anisotropic distribution over angular momenta relaxes to a Boltzmann distribution on the time scale characteristic of molecular reorientation

$$\tau^j_k \equiv \int_0^\infty \mathrm{d}tG^j_k(t)\,, \qquad (25)$$

because in the diffusion limit

$$\tau^j_k = \left\{\tau_J\left(j(j+1)-k^2\right)\right\}^{-1} \gg 1\,. \qquad (26)$$

This expression is known as the Hubbard relation [39,40,50–55,57–59]. So, in the diffusion limit, all the information concerning the photofragmentation dynamics is lost.

We further restrict ourselves to the calculation of the second rank OCF for $\vec{\mu}_1$ and $\vec{\mu}_2$ pointing along the axis of the linear photofragment, because such a situation is of a considerable practical significance [20–36]. In this case

$$r(t) = 2/5G^2_{00}(t)\,. \qquad (27)$$

The solution of Eq. (18) for $G^2_{00}(t)$ in case of an arbitrary collision frequency z_c is quite complicated task (see Appendix). The final result is however rather simple and compact: the Fourier image of the OCF can be calculated according to the following three-term recurrence relations for coefficients b_m:

$$\tilde{G}^2_{00}(\omega) \equiv \int_0^\infty \mathrm{d}t\exp\{-i\omega t\}G^2_{00}(t) = \left(1+2\sqrt{6}\,b_0\right)/i\omega\,, \qquad (28)$$

$$\frac{16(m+2)}{\sigma_{m+1}}b_{m+1} - \left\{\frac{8m+10}{\sigma_{m+1}} + \frac{8m+6}{\sigma_m} + \zeta_m\right\}b_m + \frac{4m}{\sigma_m}b_{m-1} = -\frac{\sqrt{6}}{2}\left\{\frac{\zeta_{m+1}}{\sigma_{m+1}} - \frac{\zeta_m}{\sigma_m}\right\}, \qquad (29)$$

where the explicit expressions for coefficients $\sigma_m, \varsigma_m, \zeta_m$ are given by Eq. (A13) and (A15). The calculation of $\tilde{G}^2_{00}(\omega)$ from such recursive relations is very effective and rapidly convergent routine (see Ref. [60] for general discussion). In order to get $G^2_{00}(t)$ in the time domain, the inverse Fourier transform must also be performed numerically. While

equilibrium initial conditions (10) are assumed, $\zeta_m \equiv \delta_{m0}$, and recursive formulas (29) can be solved in terms of a continued fraction. The result generalizes the approach developed by Sack [54] for the calculation of the first order OCF.

4. Results and discussion

In the present approach, the rotational motion of fragments is governed by the following four parameters: ν_J, γ, η, and Δ. The first two parameters specify dynamics of collisions of fragments and buffer species, and the last two parameters reflect the photofragmentation dynamics. The time dependencies of $G_{00}^2(t)$ for various values of these parameters are presented in Figs. 1 and 2. The solid curves correspond to the equilibrium ensemble of linear rotors. Under the collision free conditions $\nu_J \ll 1$ and in case of the large applied torque ($\Delta \gg 1$), OCFs (23) evidently reduce to

$$G_{00}^1(t) = \cos(\Delta t), G_{00}^2(t) = (1 + 3\cos(2\Delta t))/4 . \quad (30)$$

These functions are periodic with the period $\mathcal{T}^j = 2\pi : j\Delta$, $j = 1,2$. When $\Delta \gg 1$, the short time behavior for OCFs is determined by the applied torque, and peculiarities of the collision dynamics (ν_J, γ) are of minor importance, because it is no time for collisions to completely destroy these oscillations. So, a few characteristic periodic features are transparently seen in the dotted curves ($\Delta = 3$, $\mathcal{T}^2 \approx 1.05$). It should be pointed out that the inverse proportionality of the oscillation period $\mathcal{T}^j$ and the OCF rank j is accidental, because it holds true for $j = 1,2$ only. For instance, when $j = 3$ and $\Delta \gg 1$

$$G_{00}^3(t) = \{5\cos(3\Delta t) + 3\cos(\Delta t)\}/8 . \quad (31)$$

Evidently, $\mathcal{T}^3 = 2\pi/\Delta$.

Additional angular momentum Δ manifests itself characteristically in the OCF spectra, viz. $\tilde{G}_{00}^2(\omega)$ possesses a pronounced far wing shoulder (Fig. 3). In polar liquids, the very similar feature is a direct consequence of the librational motion of a molecule in the cage of its nearest neighbors, and the frequency corresponding to this shoulder is a characteristic librational frequency [40,61–64]. In our case, as it is evident from Eq. (30), $\omega_{\max}^j \approx j\Delta$, $j = 1,2$. So, examining OCFs both in the time and frequency domain allows one to estimate the additional angular momentum Δ. However, the procedure must be carried out with some caution. The point is that one must be sure that $\Delta \gg 1$. What is actually a criterion for fulfilling this strong inequality, depends, among

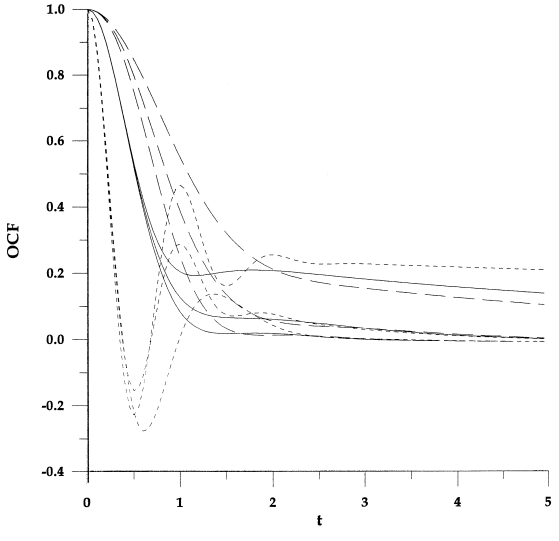

Fig. 1. Time development of the second rank OCF, $\nu_J = 1$. Solid lines are used for $\eta = 0.5$, $\Delta = 0$ (equilibrium conditions), dashed lines for $\eta = 2$, $\Delta = 0$, dotted lines for $\eta = 2$, $\Delta = 3$. In the vicinity of the point $t = 1.5$, from top to bottom, the curves correspond to $\gamma = -0.9$, $\gamma = 0$, and $\gamma = 1$.

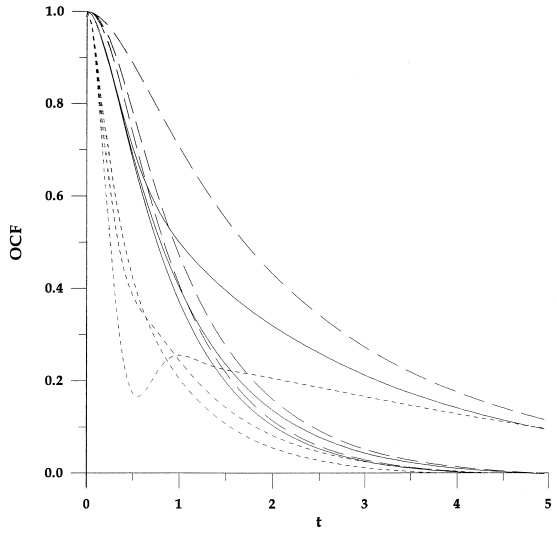

Fig. 2. Same as in Fig. 1 but for $\nu_J = 5$.

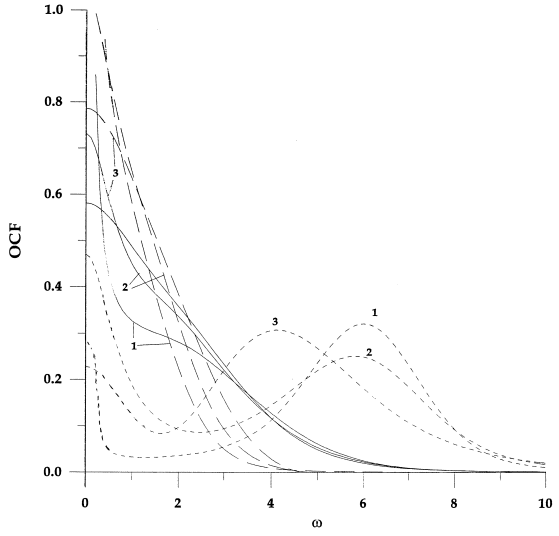

Fig. 3. Fourier spectrum of the second rank OCF, $\nu_J = 1$. Solid lines are used for $\eta = 0.5$, $\Delta = 0$ (equilibrium conditions), dashed lines for $\eta = 2$, $\Delta = 0$, dotted lines for $\eta = 2$, $\Delta = 3$. (1) stands for $\gamma = -0.9$, (2) for $\gamma = 0$, and (3) for $\gamma = 1$.

other things, on the collision dynamics. This statement is immediately illustrated by Figs. 1–3. Indeed, in case of $\gamma = -0.9$ (angular momentum reorienting collisions) and $\gamma = 0$ (strong collisions) one observes oscillations of the OCFs with the period $\mathcal{T}^2 = \pi/\Delta$ (Figs. 1 and 2) and maximums of the OCF spectra at $\omega_{\max}^2 = 2\Delta$ (Fig. 3). However for $\gamma = 1$ (weak collisions) the oscillation periods and maximums of spectra are shifted from the values given above (Figs. 1–3). To put it differently, if the transmitted torque is not high enough, a complex interplay between dissociation and relaxation results in more sophisticated behavior for OCFs. So, one should actually perform fitting of experimental and theoretical curves, to be convinced that oscillations of OCFs are indeed due to the transmitted angular momentum Δ.

While the primarily origin of the fragment rotation is that of the parent molecules ($\Delta \ll 1$), orientational relaxation can considerably slow down: according to Eq. (3), the product angular momentum is scaled by the factor $\eta^{-1/2}$ (the dimensionless quantity $\eta \equiv I_A T_{eq}/(2T_A I_B)$ is introduced in Eq. (21)). For example, $\sqrt{\langle J^2 \rangle} = \eta^{-1/2}$. So, when the parent molecules are considerably more massive than the product ones ($I_A \gg I_B$) or when $T_{eq} \gg T_A$, the product angular momentum is quite small. This is the reason of the orientational relaxation slowing down (compare solid and dotted curves in Figs. 1 and 2).

By the method described in Refs. [55,65], starting from Eq. (A7) one can conveniently calculate the first few terms of the Tailor expansion for OCF:

$$G_{00}^{j}(t) = 1 - j(j+1)(1-2\zeta_1)t^2/2! + j(j+1)\nu_J(1-2\zeta_1[2+\gamma])t^3/3! + O(t^4) \quad (32)$$

$$-\infty < \zeta_1 = 1/2 - 1/(4\eta) - \Delta^2/4 \le 1/2\,. \quad (32')$$

It is well known from the analysis of the orientational relaxation under equilibrium conditions that the coefficient near t^2 in the Tailor expansion for OCFs of colliding molecules coincides with that for OCFs of free rotors, reflecting thereby that a molecule rotates freely at a short enough time interval after a collision [37–40]. The coefficient near t^3 is completely determined by the angular momentum relaxation frequency ν_J [40,55]. Further, provided that ν_J is fixed, the higher is the angular momentum reorientation due to a collision (the closer is γ to -1) the slower is orientational relaxation [55,65]. These expectations are certainly confirmed by Eq. (32) being specialized to equilibrium conditions ($\eta = 1/2$, $\Delta = 0$, $\zeta_1 = 0$), see also Figs. 1 and 2, solid curves. When nonequilibrium initial conditions (6) are presumed, the situation is very different. On explicitly rewriting Eq. (32) as

$$G_{00}^{j}(t) = 1 - j(j+1)\left(\eta^{-1} + \Delta^2\right)t^2, 4 + O(t^3) \quad (33)$$

one sees that there exists no free rotor initial behavior. However, the rank dependence of the term is essentially the same as in case of a free rotor, so that the quantity $\sqrt{(\eta^{-1} + \Delta^2)/2}$ can be regarded as the effective photofragment temperature. When η increases ('rotational cooling') orientational relaxation slows down. When Δ increases the initial decay hastens (Figs. 1 and 2). Further, by considering the third term in Eq. (32) it is possible to infer the following observations. In case of no torque ($\Delta = 0$) and $\eta > 1/2$, one can state that the higher is the angular momentum collisional reorientation, the slower runs orientational relaxation (Figs. 1 and 2, dotted lines). On the contrary, when the torque is

high enough, the opposite situation occurs: the greater is γ (the closer molecular rotation resembles the Fokker–Planck limit) the greater is OCF (Figs. 1 and 2, dashed lines). For an ensemble of rotors under equilibrium conditions ($\eta = 1/2, \Delta = 0, \zeta_1 = 0$), the third (and also the fourth [55]) term in Tailor expansion of OCF is essentially independent of the collision efficiency γ. Summarizing, one can characterize the short time behavior for OCF as a competition between 'reality' (intermolecular collisions) and 'memory' (dynamics of the photofragmentation). It is remarkable and very helpful for practical applications that the peculiarities of the photofragmentation manifest themselves markedly not only at a short but also at the long time behavior for OCFs (compare the corresponding solid, dotted, and dashed curves in Figs. 1 and 2).

The long time behavior for OCFs transparently manifests itself in the orientational relaxation times (ORTs) τ_k^j, because these quantities are defined as integrals of OCFs over the entire time domain (Eq. (25)). In fact, ORTs can be regarded as anisotropy dephasing times. It is a popular procedure to investigate τ_k^j vs. the angular momentum relaxation time τ_J [40,53,59] or, that is equivalent, vs. the angular momentum relaxation frequency $\nu_J \equiv \tau_J^{-1}$. For equilibrium ensembles, it is a direct consequence of the above analyses for OCFs that the less is γ the more is τ_k^j (Fig. 4). The distinction between ORTs corresponding to different γ is more pronounced in the dilute gas limit. Due to the universal Hubbard relations (26), ORTs in the hindered rotation limit are independent of γ and completely determined by τ_J (Fig. 4). A very similar behavior is established when the bulk part of the fragment rotational excitation is due to the parent molecule rotation (Fig. 4, dotted curves). In the dilute gas limit ($\nu_J \leq 1$), these ORTs are less than equilibrium ORTs. While ν_J increases, the opposite behavior is observed (Fig. 4). So, high enough values of ORTs in the hindered rotation limit could be indicative not only of a substantial angular momentum collisional reorientation, but also of 'rotational cooling'. When a substantial torque is imparted on the fragment, an inverse situation takes place. The so calculated ORTs are greater than equilibrium ORTs in the dilute gas limit. If ν_J increases, the torque manifests itself in a considerable reduction of the ORT value (Fig. 4). When collisions do not reverse the photoproduct angular momentum ($\gamma \geq 0$) and $\nu_J \sim 1$ (intermediate densities) ORTs are tangibly less than their equilibrium counterparts. Moreover, the ORTs values turn out to be significantly less then the minimal values of ORTs under equilibrium conditions, that correspond to the Fokker–Planck limit of molecular collisions [40,55,66,67]. So, the photofragmentation considerably expands the 'corridor' of the allowed values of ORTs as compared with that for equilibrium conditions [40,67].

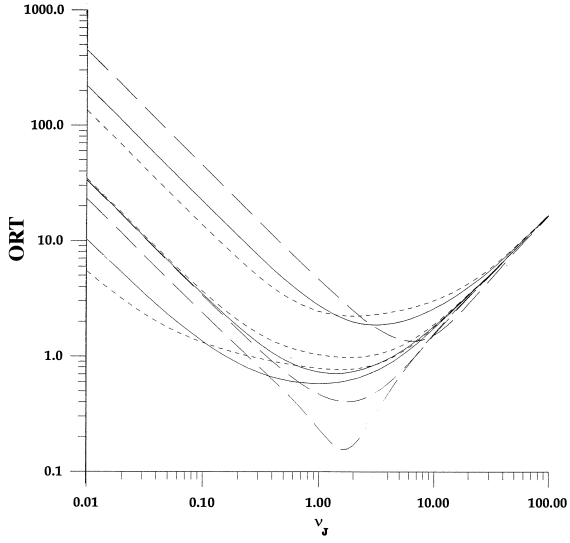

Fig. 4. The second rank ORT vs. ν_J. Solid lines are used for $\eta = 0.5$, $\Delta = 0$ (equilibrium conditions), dashed lines for $\eta = 2$, $\Delta = 0$, dotted lines for $\eta = 2$, $\Delta = 3$. In the vicinity of the point $\nu_J = 1$, from top to bottom, the curves correspond to $\gamma = -0.9$, $\gamma = 0$, and $\gamma = 1$.

Now we shall try to apply the developed approach to the interpretation of the experimental data of the Hocstrasser's group on dissociation of HgI_2 in ethanol for 270-nm pump and 490-nm probe [30,31]. First, we fit the results of the equilibrium molecular dynamics simulations for diatomic *HgI* at 300 K ($\tau_r = 1.5$ ps). As it is described above, we choose the angular momentum relaxation frequency $\nu_J = 3.5$ to ensure the short time coincidence of the simulated and calculated OCFs. After so doing, we vary γ to adjust the curves at latter times. The results are depicted in Fig. 5, where $\gamma = -0.93$ is seen to provide excellent coincidence of the OCFs (all the

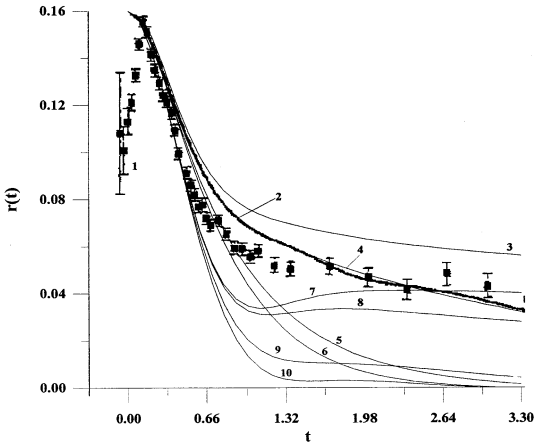

Fig. 5. Comparison of the calculated and simulated anisotropy decays for *HgI*. (1) for experimental measurements; (2) for equilibrium molecular dynamics simulations at 300 K. Curves 3–6 correspond to $\eta = 0.5$, $\Delta = 0$, $\nu_J = 3.5$. (3) stands for $\gamma = -0.999$; (4) for $\gamma = -0.93$; (5) for $\gamma = 0$; (6) for $\gamma = 1$. Curves 7–10 correspond to $\eta = 0.5$, $\Delta = 0$, $\nu_J = 1$. (7) stands for $\gamma = -0.99$; (8) for $\gamma = -0.9$; (9) for $\gamma = 0$; (10) for $\gamma = 1$. Curves 1 and 2 are taken from Ref. [31].

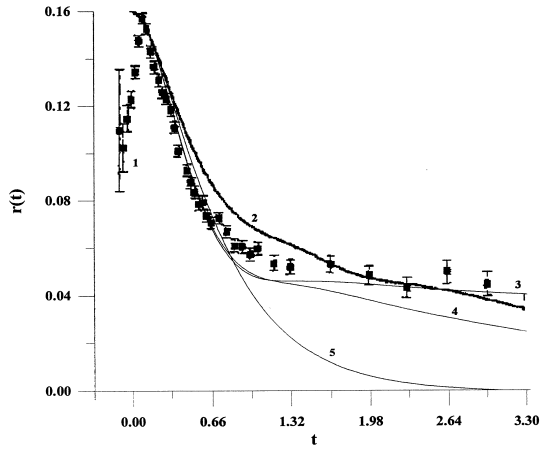

Fig. 6. Comparison of the calculated and experimental anisotropy decays for *HgI*. (1) for experimental measurements; (2) for equilibrium molecular dynamics simulations at 300 K. Curves 3–5 correspond to $\nu_J = 3.5$, $\Delta = 1.4$; (3) $\gamma = -0.99$, (4) $\gamma = -0.9$, (5) $\gamma = 1$. Curves 1 and 2 are taken from Ref. [31].

calculated OCFs are scaled to yield $G^2_{00}(0) = 0.16$). This value of γ corresponds to a considerable reorientation of the angular momentum due to a collision. This fact is indicative of the quasilibrational character of the molecular rotation in liquids, that is confirmed by a number of computer simulations, including those reported in [30,31]. It is very important for the further analyses, that we were unable to perform the above mentioned fitting procedure for *HgI* produced through the photofragmentation of HgI_2. While trying to fit experimental *HgI* anisotropy by equilibrium Keilson–Storer OCFs, we can provide the short time (at $t \leq 1$) resembles of the curves ($\nu_J = 1$), but further we evidently fail to achieve a fit of theoretical and experimental curves by varying γ (Fig. 5). It is our opinion, that this is an indication of the fact that photoproducts retain their memory of the initially nonequilibrium distribution over angular momenta, despite of quite frequent collisions with buffer spices. To confirm this observation, we attempted to adjust experimental anisotropies by nonequilibrium Keilson–Storer OCFs. For the experiment described in [30,31] one should assume that $T_{eq} = T_A$, so that the dimensionless parameter η is entirely determined by the ratio of the parent and product moments of inertia: $\eta = 1729/(2 \times 529) = 1.63$. In a trial to fit the experimental anisotropy one is allowed to vary ν_J, γ and Δ. The results of this procedure are depicted in Figs. 6 and 7. By taking $\nu_J = 3.5$ (as in the case of equilibrium conditions) experimental anisotropies are fitted reasonably well by $\gamma = -0.99$, $\Delta = 1.4$ (Fig. 6). However, a better fit one gets for $\nu_J = 8$, $\gamma = -0.99$, $\Delta = 2$ (Fig. 7). Note that the measured anisotropy exhibits a small scale oscillations that originate from the vibrational modulation of the interatomic length. These oscilla-

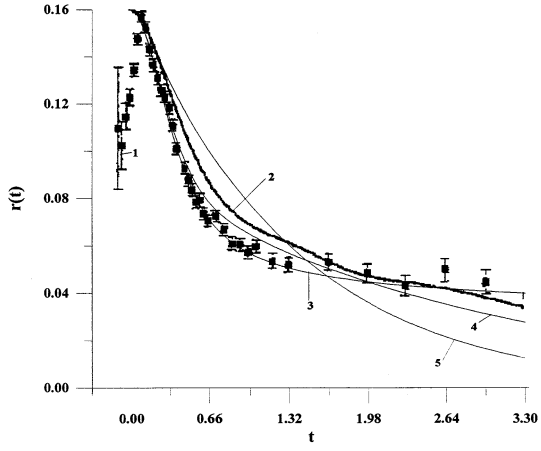

Fig. 7. Same as in Fig. 6 but for $\nu_J = 8$, $\Delta = 2$.

tions certainly can not be reproduced within the assumption that the fragment is a rigid body. Such a large scale scatter of parameters ν_J and Δ is explained by formulas 32) and (33). A simultaneous increase of ν_J and Δ does not result in alternations of the short time decay for the OCF. So the fitting procedure should be carried out more carefully. Nonetheless, a high degree of the angular momentum reorientation should be stressed, because it is the same for both sets of fitting parameters. Note that the values of parameters η and Δ, that are used here to adjust the experimental results [30,31], differ markedly from those determined in [22] for the same reaction under collisionless conditions. Evident explanations for this discrepancy are as follows. First, nonequilibrium distribution [17] is distinguished from the shifted Gaussian $\rho_0^{\text{Gauss}}(J) \sim \exp\{((J - J_0)/\Delta_J)^2\}$ used in [22], where J_0 and Δ_J were taken as high as 80 and 90, respectively. Second, the influence of the surrounding molecules can show itself in a significant alternation of the parameters. Third, and by all means the most important reason is that the authors of paper [22] performed averaging of the free rotor OCF (22) either over $\int_0^\infty J\mathrm{d}J\rho_{\text{eq}}(J)\ldots$ or over $\int_0^\infty \mathrm{d}J\rho_0^{\text{Gauss}}(J)\ldots$ Both $J\rho_{\text{eq}}(J)$ and $\rho_0^{\text{Gauss}}(J)$ reach their maxima at some $J_{\max} \neq 0$, that allows one to reproduce the observed anisotropy deep [22]. So J_0, that is the analogue of our Δ, can not be regarded as the transferred angular momentum, because just the same behavior for the anisotropy decay can be modeled by an equilibrium distribution $J\rho_{\text{eq}}(J)$, i.e., with $J_0 \equiv 0$. According to the present analyses, the averaging should be done over $\int_0^\infty J\mathrm{d}J\rho_0(J)\ldots$ It is in this case Δ can be considered as the transmitted angular momentum.

The results of the comparison of the present theory and computer simulations of the reaction $I_3^- + h\nu \rightarrow I_2^- + I$ in ethanol at 295 K [34] are presented in Fig. 8. In this case $T_{\text{eq}} = T_A$, $\tau_r = 1.5$ ps, and $\eta \equiv 2$. The equilibrium OCF for I_2^- is satisfactory fitted by the equilibrium Keilson–Storer OCF with $\nu_J = 10.3$, $\gamma = -0.96$. The behavior for the iodine ion OCF after the photofragmentation is reasonably well adjusted by the curve corresponding to the same collision parameters $\nu_J = 10.3$, $\gamma = -0.96$, and the acquired angular momentum $\Delta = 1.7$. So, one can conclude that the collision dynamics is relatively insensitive to the photofragmentation (ν_J, γ), while

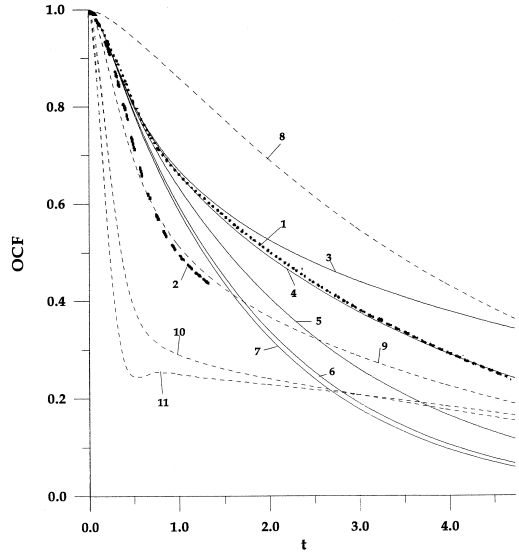

Fig. 8. Comparison of the calculated and simulated anisotropy decays for I_2^-. (1) I_2^- equilibrated in ethanol at 295 K; (2) I_2^- in ethanol following I_3^- photodissociation. Curves 3–7 correspond to $\nu_J = 10.3$, $\eta = 1/2$, $\Delta = 0$. (3) $\gamma = -0.99$; (4) $\gamma = -0.96$; (5) $\gamma = -0.8$; (6) $\gamma = 0$; (7) $\gamma = 1$. Curves 8–11 correspond to $\nu_J = 10.3$, $\eta = 2$, $\gamma = -0.96$. (8) $\Delta = 0$; (9) $\Delta = 1.7$; (10) $\Delta = 3$, (11) $\Delta = 4$. Curves 1 and 2 are taken from Ref. [34].

the latter manifests itself through the nonequilibrium initial conditions (η and Δ). In Fig. 1 of paper [34], the time relaxation of the rotational energy is depicted. The dependence was found to be nearly time independent, that was indicative of

$$\langle \vec{J}^2 \rangle \approx \langle \vec{J}^2 \rangle_{\text{eq}}, \tag{34}$$

(see Eq. (13)). It is a direct consequence of the present analyses, that the requirement (34) is not a manifestation of the fact that I_2^- is produced with an equilibrium distribution. Indeed, by invoking explicit formulas (14), one finds that Eq. (34) is obeyed for $\Delta^2 \approx 2 - \eta^{-1}$. It is only in the case $\eta = 1/2$ ($I_A = I_B$, in fact, no dissociation takes place) Eq. (34) results in $\Delta = 0$. Otherwise, Eq. (34) predicts $\Delta \neq 0$. For $\eta = 2$, one obtains $\Delta = 1.2$. This is in the order of magnitude in a correspondence with the value of Δ used for the fitting of the simulated OCFs.

Of course, we can not definitely ascertain that the dynamic parameters ν_J, γ and Δ listed above are the 'actual' parameters for the $HgI_2 + h\nu \rightarrow HgI + I$ and $I_3^- + h\nu \rightarrow I_2^- + I$ reactions. However, the main find-

ing of the present work is that the photoproduct anisotropy decay in collisional environments does contain information both of the photofragmentation and collision dynamics, which can be extracted by an appropriate theoretical analysis.

In this paper, no attempt was made to fit anisotropies of CO fragments produced through photodissociation from heme [23–25], since external confining potentials contribute significantly into the fragment dynamics and result in an appreciable retardation of the fragment reorientation. We merely would like to point out that, in principle, a considerable slowing down of the fragment rotation can have not only a static origin (confining potentials), but also a dynamic origin ($I_A \gg I_B$, see Eq. (3)).

5. Conclusion

In this paper, a simple approach is developed for the investigation of the photofragment anisotropy decay. The approach treats the photofragmentation as an instantaneous process, which produces photoproducts with a nonequilibrium rotational distribution which father relaxes to an equilibrium due to collisions of fragments with buffer species. The theory presented here can (and should) be further improved to a more realistic description of the photofragmentation dynamics (predissociation, cage effects) and of the fragment rotational dynamics (non-Markovian effects). However, the main result of the present analyses can be formulated as follows. The time evolution of the photoproduct anisotropy is very sensitive both to the collision and photofragmentation dynamics. This is pertain not only to the short time behavior for the anisotropy, but also for its long time decay.

Acknowledgements

This work was supported in part by Grant F96-160 from the Foundation for Basic Researches of Belarus. We would like to thank Prof. A.I. Burshtein for sending us the second edition of his book (Ref. [40]). M.G. is grateful to Dr. A. Borodich for helpful discussions.

Appendix A

In order to solve Eq. (17) subjected to initial condition (18), it is convenient to introduce the Fourier transformed function

$$H^j_{kl}(\vec{u},t) = \exp\{u^2/2\}\int_{-\infty}^{\infty} \mathrm{d}\vec{J}\exp\{-i\vec{u}\vec{J}\}G^j_{kl}(\vec{J},t)\,, \tag{A1}$$

(compare with [54,55,65]). Evidently,

$$G^j_{kl}(t) \equiv H^j_{kl}(0,t)\,. \tag{A2}$$

On taking the Fourier transformation of Eq. (17), one gets

$$\partial_t H^j_{kl}(\vec{u},t) = \sum_{m=-j}^{j}\left(\partial_{\vec{u}} - \vec{u}\right)\vec{J}^j_{km}H^j_{lm}(\vec{u},t) - z_c H^j_{kl}(\vec{u},t) + z_c H^j_{kl}(\gamma\vec{u},t)\,. \tag{A3}$$

The initial condition for this equation reads

$$H^j_{kl}(\vec{u},0) = \exp\{(2\eta-1)u^2/4\eta\}J_0(u\Delta)\,\delta^j_{kl}\,, \tag{A4}$$

where $J_o(z) = I_o(\mathrm{i}z)$ is the Bessel function. Eq. (A4) evidently depends only upon the magnitude of vector $\vec{u}$, but not upon its direction. Keeping this fact in mind, it is convenient to introduce the polar coordinates

$$u_x = u\cos\varphi_u,\; u_y = u\sin\varphi_u\,. \tag{A5}$$

After so doing, one can immediately verify that

$$H^j_{kl}(\vec{u},t) = \exp\{-\mathrm{i}\varphi_u(k-l)\}h^j_{kl}(u,t), h^j_{kl}(u,t) \equiv h^j_{-k-l}(u,t)\,, \tag{A6}$$

(to establish these identities, the explicit form (19) of the matrix elements over *D*-functions was used). On inserting (A6) into (A3), one finds

$$\partial_t h^j_{kl}(u,t) = \sum_{\pm}\lambda_{\pm}(k)\left(\partial_u + [1\pm(k-l)]/u - u\right)h^j_{k\pm1,l}(u,t) - z_c h^j_{kl}(u,t) + z_c h^j_{kl}(\gamma u,t)\,, \tag{A7}$$

$$\lambda_{\pm}(k) = \sqrt{(j\mp k)(j\pm k+1)}\,,$$

$$h^j_{kl}(u,0) \equiv H^j_{kl}(\vec{u},0), G^j_{kl}(t) \equiv h^j_{kl}(0,t)\,. \tag{A8}$$

On taking the Fourier transformation of Eq. (A7) over the time variable, one arrives at the equivalent equation

$$
\begin{aligned}
&-h^j_{kl}(u,0) + \mathrm{i}\omega\tilde{h}^j_{kl}(u,\omega) \\
&\quad = \sum_{\pm} \lambda_{\pm}(k)\left(\partial_u + \left[1 \pm (k-l)\right]\right. \\
&\qquad \left./u - u\right)\tilde{h}^j_{k\pm 1,l}(u,\omega) - z_c\tilde{h}^j_{kl}(u,\omega) \\
&\qquad + z_c\tilde{h}^j_{kl}(\gamma u,\omega)\,, \qquad \text{(A9)}
\end{aligned}
$$

where

$$
\tilde{h}^j_{kl}(u,\omega) \equiv \int_0^\infty \mathrm{d}t \exp\{-\mathrm{i}\omega t\} h^j_{kl}(u,t)\,. \qquad \text{(A10)}
$$

In order to solve Eq. (A9) for $\tilde{h}^2_{00}(0,\omega) \equiv \tilde{G}^2_{00}(\omega)$, one should put $l = 0$ and seek for the solution in the following form:

$$
\begin{aligned}
\tilde{h}^2_{00}(u,\omega) &= \sum_{m=0}^{\infty} a_m u^{2m}/m!\,, \\
\tilde{h}^2_{10}(u,\omega) &= \sum_{m=0}^{\infty} b_m u^{2m+1}/m!, \tilde{h}^2_{00}(u,\omega) \\
&= \sum_{m=0}^{\infty} c_m u^{2m}/m!\,. \qquad \text{(A11)}
\end{aligned}
$$

Further, one should note that

$$
\begin{aligned}
h^2_{k0}(u,0) &= \delta^2_{k0}\exp\{(2\eta-1)u^2/4\eta\} J_0(u\Delta) \\
&= \delta^2_{k0}\sum_{n=0}^{\infty}\zeta_n u^{2n}/n!\,, \\
\zeta_n &= \sum_{l=0}^{n}\left[(2\eta-1)/4\eta\right]^{n-l}\left(-\Delta^2/4\right)^l \\
&\quad \times \frac{n!}{(l!)^2(n-l)!}\,. \qquad \text{(A12)}
\end{aligned}
$$

Actually, better by far is to use, instead of Eq. (A12), the recursive formulas

$$
\begin{aligned}
&\zeta_{n+1} = \frac{(8\alpha n + 4\alpha - \beta)\zeta_n - 4\alpha^2\zeta_{n-1}}{4(n+1)^2},\ \zeta_0 = 1, \\
&\zeta_1 = \alpha - \beta/4, \\
&\alpha \equiv 1/2 - 1/(4\eta), \beta = \Delta^2\,. \qquad \text{(A13)}
\end{aligned}
$$

Eq. (13) are immediately derivable from the differential equation for the Bessel function $J_o(x)$. Now one can insert Eq. (A11) into (A9) to get the following system for coefficients a_m, b_m, c_m:

$$
\begin{aligned}
&-\zeta_m = \sqrt{6}\left\{2(m+1)b_m - mb_{m-1}\right\} - \sigma_m a_m\,, \\
&0 = \left(\sqrt{6}/2\right)\left\{2a_{m+1} - a_m\right\} + 2(m+2) \\
&\qquad /(m+1)c_{m+1} - c_m\} - \varsigma_m b_m\,, \\
&0 = 2mb_m - mb_{m-1} - \sigma_m c_m\,. \qquad \text{(A14)}
\end{aligned}
$$

Here

$$
\sigma_m \equiv \mathrm{i}\omega + z_c\left(1-\gamma^{2m}\right),\ \varsigma_m \equiv \mathrm{i}\omega + z_c\left(1-\gamma^{2m+1}\right)\,. \qquad \text{(A15)}
$$

By excluding a_m, c_m from this system, one obtains Eq. (28). By utilizing the procedure described above, one can also solve Eq. (A9) for $\tilde{\mathrm{h}}^j_{kk}(0,\omega) \equiv \tilde{G}^j_{kk}(\omega)$ with an arbitrary j and k.

References

[1] C.H. Greene, R.N. Zare, Annu. Rev. Phys. Chem. 33 (1982) 119.
[2] C.H. Greene, R.N. Zare, J. Chem. Phys. 78 (1983) 6741.
[3] R.B. Bernstein, D.R. Hershbach, R.D. Levine, J. Phys. Chem. 91 (1987) 5365.
[4] J.P. Simons, J. Phys. Chem. 91 (1987) 5378.
[5] P.L. Houston, J. Phys. Chem. 91 (1987) 5388.
[6] R. Lavi, D. Schwartz-Lavi, I. Bar, S. Rosenwaks, J. Phys. Chem. 91 (1987) 5398.
[7] J. August, M. Brouard, M.P. Docker, A. Hogson, G.J. Milne, J.P. Simons, Ber. Buns. Phys. Chem. 92 (1988) 264.
[8] F.J. Comes, K.H. Gericke, A.U. Grunewald, S. Klee, Ber. Buns. Phys. Chem. 92 (1988) 273.
[9] G.E. Hall, R.O. Loo, H.-P. Härri, N. Sivakumar, G.K. Chawla, P.L. Houston, D.W. Chandler, J.W. Hepburn, I. Burak, Ber. Buns. Phys. Chem. 92 (1988) 281.
[10] S. Klee, K.H. Gericke, F.J. Comes, Ber. Buns. Phys. Chem. 92 (1988) 420.
[11] M. Glass-Manjean, J.A. Beswick, J. Chem. Soc., Faraday Trans. 2 85 (1989) 983.
[12] R.B. Bernstein, S.E. Choi, S. Stolte, J. Chem. Soc., Faraday Trans. 2 85 (1989) 1097.
[13] T.J. Butenhoff, K.L. Carleton, M.-C. Chuang, C.B. Moore, J. Chem. Soc., Faraday Trans. 2 85 (1989) 1155.
[14] M.P. Docker, A. Ticktin, U. Brühlmann, J.R. Huber, J. Chem. Soc., Faraday Trans. 2 85 (1989) 1169.
[15] R.O. Loo, C.E. Strauss, H.-P. Härri, G.E. Hall, P.L. Houston, I. Burak, J.W. Hepburn, J. Chem. Soc., Faraday Trans. 2 85 (1989) 1185.
[16] M. Brouard, M.T. Martinez, J. O'Mahony, P. Simons, J. Chem. Soc., Faraday Trans. 2 85 (1989) 1207.
[17] F.J. Comes, Ber. Buns. Phys. Chem. 94 (1990) 1268.

[18] V.A. Povedailo, A.P. Blokhin, M.F. Gelin, V.A. Tolkachov, Opt. Spectrosc. 73 (3) (1992) 320.
[19] A.P. Blokhin, M.F. Gelin, S.A. Polubisok, V.A. Tolkachev, A.A. Blokhin, J. Mol. Struct. 408/409 (1997) 569.
[20] A. Zewail, J. Chem. Soc. Faraday Trans. 2 85 (1989) 1221.
[21] M. Dantus, R.M. Bowman, S. Baskin, A. Zewail, Chem. Phys. Lett. 159 (1989) 406.
[22] S. Baskin, A. Zewail, J. Phys. Chem. 98 (1994) 3337.
[23] J.E. Straub, M. Karplus, Chem. Phys. 158 (1991) 221.
[24] B. Locke, T. Lian, R.M. Hochstrasser, Chem. Phys. 158 (1991) 409.
[25] M. Lim, T.A. Jackson, P.A. Anfinrud, J. Chem. Phys. 102 (1995) 4355.
[26] U. Banin, A. Waldman, S. Ruhman, J. Chem. Phys. 96 (1992) 2416.
[27] U. Banin, S. Ruhman, J. Chem. Phys. 98 (1993) 4391.
[28] E. Lenderink, K. Duppen, D.A. Wiersma, Chem. Phys. Lett. 211 (1993) 503.
[29] C. Wan, M. Gupta, A. Zewail, Chem. Phys. Lett. 256 (1996) 279.
[30] S. Gnanakaran, M. Lim, N. Pugliano, M. Volk, R.M. Hochstrasser, J. Phys.: Condense Matter 8 (1996) 9201.
[31] M. Volk, S. Gnanakaran, E. Gooding, Y. Kholodenko, N. Pugliano, R.M. Hochstrasser, J. Phys. Chem. A 101 (1997) 638.
[32] M. Lim, S. Gnanakaran, R.M. Hochstrasser, J. Chem. Phys. 106 (1997) 3485.
[33] I. Benjamin, K.R. Wilson, J. Chem. Phys. 90 (1989) 4176.
[34] I. Benjamin, U. Banin, S. Ruhman, J. Chem. Phys. 98 (1993) 8337.
[35] I. Benjamin, J. Chem. Phys. 103 (1996) 2459.
[36] A.I. Krylov, B.B. Gerber, J. Chem. Phys. 100 (1994) 4242.
[37] A.J. Barnes, W.J. Orville-Thomas, J. Yarwood (Eds.), Molecular Liquids, NATO ASI Series, C, V. 135, 1984.
[38] W. Coffey, M. Evans, P. Grigolini, Molecular Diffusion and Spectra, Wiley, 1984.
[39] W.G. Rothschild, Dynamics of Molecular Liquids, New York, Wiley, 1984.
[40] A.I. Burshtein, S.I. Temkin, Spectroscopy of Molecular Rotations in Gases and Liquids, Cambridge University Press, Cambridge, 1994.
[41] M.P. Allen, D.J. Tildesley, Computer Simulation of Liquids, Clarendon Press, Oxford, 1989.
[42] A.P. Blokhin, M.F. Gelin, Opt. Spectrosc. 77, (2) (1994) 32, 200.
[43] A.P. Blokhin, M.F. Gelin, Opt. Spectrosc. 74 (2) (1993) 171.
[44] A.P. Blokhin, M.F. Gelin, J. Luminesc. 72/74 (1997) 840.
[45] A.P. Blokhin, M.F. Gelin, Proceedings SPIE 3090 (1997) 103.
[46] I. Hanazaki, Chem. Phys. Lett. 218 (1994) 151.
[47] H.B. Levene, J.J. Valentini, J. Chem. Phys. 87 (1987) 2594.
[48] T.J. Butenhoff, K.L. Carleton, C.B. Moore, J. Chem. Phys. 92 (1990) 377.
[49] I.-C. Chen, C.B. Moore, J. Phys. Chem. 94 (1990) 269.
[50] M. Fixman, K. Rider, J. Chem. Phys. 51 (1969) 2425.
[51] R.E.D. McClung, J. Chem. Phys. 73 (1980) 2435.
[52] J. Keilson, J.E. Storer, Quart. J. Appl. Math. 10 (1952) 243.
[53] R.E.D. McClung, Adv. Molec. Relax. Interac. Proc. 10 (1977) 83.
[54] R.A. Sack, Proc. Phys. Soc. B 70 (1957) 402, 414.
[55] A.P. Blokhin, M.F. Gelin, Molec. Phys. 87 (1996) 455.
[56] A.G. St. Pierre, W.A. Steele, Phys. Rev. 184 (1969) 172.
[57] G.T. Evans, J. Chem. Phys. 65 (1976) 3030.
[58] G.T. Evans, J. Chem. Phys. 67 (1977) 2911.
[59] J.G. Powles, G. Rickayzen, Molec. Phys. 33 (1977) 1207.
[60] H. Risken, The Fokker-Planck Equation, Berlin, Springer, 1984.
[61] R.M. Lynden-Bell, W.A. Steele, J. Phys. Chem. 88 (1984) 6514.
[62] S.K. Deb, Chem. Phys. 120 (1988) 225.
[63] A. Polimeno, G.J. Moro, J.H. Freed, J. Chem. Phys. 102 (1995) 8094.
[64] A. Polimeno, G.J. Moro, J.H. Freed, J. Chem. Phys. 104 (1996) 1090.
[65] A.P. Blokhin, M.F. Gelin, J. Phys. Chem. B 101 (1997) 236.
[66] S.I. Temkin, W.A. Steele, Chem. Phys. Lett. 215 (1993) 285.
[67] S.I. Temkin, A.I. Burshtein, J. Chem. Phys. 100 (1994) 1775.